JOURNAL OF SOLID STATE CHEMISTRY **121,** 143–148 (1996)
ARTICLE NO. 0021

Vaporization and Diffusion of Manganese–Zinc Ferrite

Hideaki Inaba

Technical Research Laboratories, Kawasaki Steel Corporation, Kawasaki-Chou, Chuo-ku, Chiba 260, Japan

and

Tsuneo Matsui

Department of Nuclear Engineering and Quantum Engineering, Graduate School of Engineering, Nagoya University, Furo-Chou, Chikusa-ku, Nagoya 464-01, Japan

Received January 18, 1995; in revised form September 11, 1995; accepted September 13, 1995

Vaporization and diffusion of Mn–Zn ferrite were studied for both powdered and bulk sintered samples by a mass-spectrometric method and EPMA analysis. Equilibrium vapor pressures were obtained using the powdered sample and the predominant vapor species was Zn(g) with small fractions of FeO(g) and MnO(g). Over the bulk sintered sample, the vapor pressures of Zn(g), FeO(g), and MnO(g) exponentially decreased with time and approached finite values. The surface was depleted severely with Zn atoms and slightly with O atoms while it was enriched with Mn and Fe atoms. The diffusion equation is solved for the Zn profile using the time-dependent boundary condition of the surface, and the diffusion profile of Zn is analyzed. The activation energy of diffusion obtained is 410 kJ mol^{-1}, which is about three times larger than the literature value obtained by the tracer method.

I. INTRODUCTION

Manganese–zinc ferrites have been widely used in electronic applications such as transformers, choke coils, noise filters, and recording heads, because of their high magnetic permeabilities and low magnetic losses. It is widely known (1–6) that the vaporization loss of Zn during sintering depresses the magnetic properties of Mn–Zn and Ni–Zn ferrites. However, only a few studies have been conducted on the direct observation of vapor species (1, 2) and the diffusion profiles of Zn atoms (3). It has been shown (1, 2) that the vaporization of Zn occurs in the form of Zn(g) and the vapor pressure of Zn(g) is one or two orders magnitude larger than those of MnO(g) and FeO(g). When the predominant vaporization of Zn occurs from the surface of the sample, compositional rearrangement and diffusion subsequently occur due to differing compositions of Fe, Mn, Zn, and O between the surface and bulk. Not only for practical but also for physico-chemical interest it is important to know the behaviors of the vapor and of the diffusing species of the solid using the same sample. Since the dynamic vaporization and diffusion behavior of Mn–Zn ferrits is considered to depend on the size and shape of sample, it is desirable to use both the powdered sample and the bulk sintered samples for vaporization and diffusion studies.

In this study, vaporization has been studied for both the powdered and the bulk sintered samples and diffusional analysis in relation to the vaporization kinetics has been made for the latter sample.

II. EXPERIMENTAL PROCEDURE

Manganese–zinc ferrites having the formula $Mn_{0.676}Zn_{0.261}Fe_{2.063}O_4$ were prepared by the usual ceramic techniques. The mixture of α-Fe_2O_3, Mn_3O_4, and ZnO in an appropriate metal composition was mixed in a ball-mill, prefired for 1 hr at 1173 K, then ground to obtain 1.2 μm powder in a ball-mill adding 550 ppm of $CaCO_3$ and 100 ppm of SiO_2. Finally the sample was pressed into the shape of a bar. The pressed samples were heated to 1373 K in a box-type furnace at a rate of 200 K h^{-1} under an air atmosphere, then to 1593 K under the oxygen partial pressure of 0.03 atm. The samples were then sintered by being kept 3 hr at 1593 K under the same oxygen partial pressure, and then cooled at the rate of 200 K h^{-1} to 1373 K, then under an atmosphere of nitrogen gas flow below 1373 K. The oxygen partial pressure was controlled by flowing a mixture of oxygen and nitrogen gases with a fixed ratio using mass flow controllers and was also determined by a nonstoichiometric cobaltous oxide sensor calibrated in our laboratory before use. The sintered bar was cut into a rectangular prismatic shape with a base of 4 × 3 mm and a height of 6 mm. The powdered sample was obtained by

0022-4596/96 $12.00

grinding the sintered bar. The average grain size for the bulk sintered polycrystalline sample was determined as 8.6 μm from the photograph of a microscope using the sample chemically etched by hot HCl. The average particle diameter of the powder sample was determined as 12 μm from a photograph taken by a scanning electron microscope. The bulk sintered sample was polished to a roughness of about 2 μm, annealed at 1473 K for 1.5 hr in air and then quenched to room temperature. The two powdered samples were annealed at different conditions, one at 1473 K for 1.5 hr in air and the other at 1393 K for 3 hr in a controlled oxygen pressure of 5.0 Pa. Then they were quenched to room temperature in the respective atmospheres in order to control the oxygen stoichiometry (7, 8). The amount of Fe^{2+} and total Fe for these samples was determined by chemical analysis (9, 10) with the estimated error of 0.06%. The ratio of Fe^{2+} to total Fe in the samples annealed in air and that annealed in an oxygen pressure of 5.0 Pa were obtained as $(5 \pm 5) \times 10^{-4}$ and 0.030 ± 0.001, respectively. The Mn and Zn contents were also determined by chemical analysis (11, 12) with estimated error of 0.06%. The composition of the sample can thus be written as $Mn_{0.676}Zn_{0.261}Fe_{2.063}O_{4.031}$ and $Mn_{0.676}Zn_{0.261}Fe_{2.063}O_{4.000}$, respectively, using the equation for the nonstoichiometry of Mn–Zn ferrites given by Morineau and Paulus (7). The X-ray diffraction pattern for these samples showed a cubic spinel phase with lattice constants 0.8496 and 0.8498 nm, respectively.

The vapor pressure was measured with a time-of-flight mass spectrometer equipped with a zirconia Knudsen cell in a tungsten holder heated by electron bombardment. The electron energy used to ionize the gaseous species was 18 eV. The absolute pressure was determined by comparing the intensity of the ionic current of the vapor species with that of silver gas over silver metal as a standard. The values of the atomic ionization cross sections of Ag, O, Fe, Mn, and Zn were taken from Mann (13). The additivity principle suggested by Otvos and Stevenson (14) was used to calculate the molecular cross sections of MnO, ZnO, and FeO. Temperature measurements in the vaporization study were made with a Leeds and Northrup disappearing-filament optical pyrometer, for which the error was within ± 5 K. Observation was made through an orifice of the Knudsen cell. Each experimental run, where normally two or three data points were taken for one batch of powdered sample, was carried out within 1–2 hr. On the other hand, the experiments were conducted up to 6 hr for the rectangular prismatic samples.

The depth profiles of Zn, Mn, Fe, and O atoms were observed for the vertical section of the rectangular prism by using an Electron Probe Micro-Analyzer (EPMA). The line-analysis of the EPMA was made with a voltage of 15 kV, and a beam current of 50 nA; the diameter of the beam was about 1 μm and the scan speed was 25 μm min^{-1}.

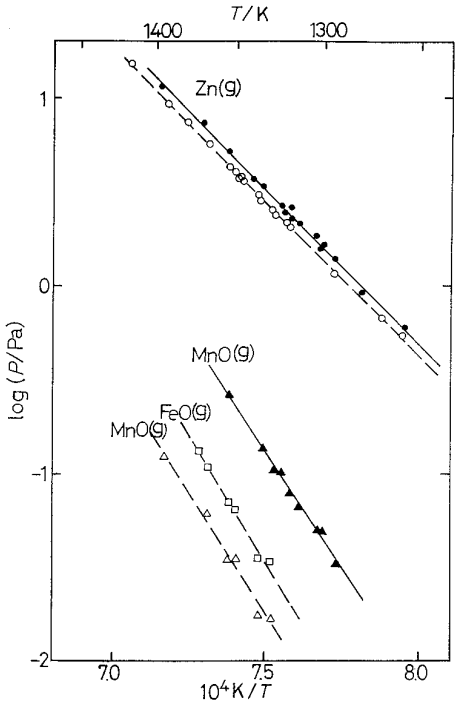

FIG. 1. Temperature dependence of the vapor pressures of Zn(g), FeO(g), and MnO(g) over $Mn_{0.676}Zn_{0.261}Fe_{2.063}O_{4+\delta}$ powdered samples (solid line) $\delta = 0.000$; (broken line) $\delta = 0.031$.

III. RESULTS

The partial vapor pressures of Zn(g), FeO(g), and MnO(g) over the powdered sample of $Mn_{0.676}Zn_{0.261}Fe_{2.063}O_{4.031}$ and those of Zn(g) and MnO(g) over $Mn_{0.676}Zn_{0.261}Fe_{2.063}O_{4.000}$ are shown as a function of the reciprocal temperature in Fig. 1 (1, 2). The partial vapor pressures over the powdered sample did not change significantly during measurement and the weight change of the sample was within experimental error. Partial vapor pressures over $Mn_{0.676}Zn_{0.261}Fe_{2.063}O_{4.031}$ decreased on order of Zn(g), FeO(g), and MnO(g), and the partial pressure of Zn(g) was one or two orders of magnitude larger than those of FeO(g) and MnO(g) over the temperature range of this measurement. In the case of $Mn_{0.676}Zn_{0.261}Fe_{2.063}O_{4.000}$, the partial vapor pressure of Zn(g) was also larger than that of MnO(g). The partial vapor pressure of FeO(g) over $Mn_{0.676}Zn_{0.261}Fe_{2.063}O_{4.000}$ could not be experimentally measured in this study, since its vapor pressure is lower than the detection limit of our mass spectrometer. These facts indicate that Mn–Zn ferrites do not vaporize congruently and the composition of Mn–Zn ferrites shifts to the lower Zn content with time at the surface.

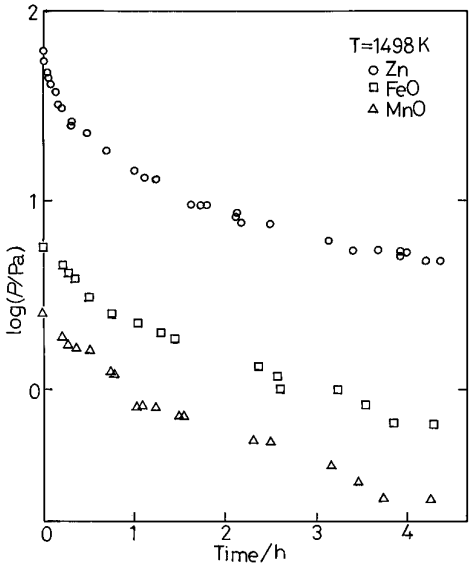

FIG. 2. Vapor pressures of Zn(g), FeO(g), and MnO(g) over the bulk sintered sample $Mn_{0.676}Zn_{0.261}Fe_{2.063}O_{4.031}$ as a function of time at 1498 K.

The partial vapor pressures of Zn(g), FeO(g), and MnO(g) over the rectangular prismatic sample of $Mn_{0.676}Zn_{0.261}Fe_{2.063}O_{4.031}$ are shown as a function of time at 1498 and 1603 K in Figs. 2 and 3, respectively. The vapor pressures seem to decrease exponentially at first and then approach steady state values. Although the magnitudes of the vapor pressures of Zn(g), FeO(g), and MnO(g) differ from each other, the time dependence of vapor pressures was quite similar among them. The slope of the vapor pressures versus time curve at 1498 K was larger than that at 1603 K.

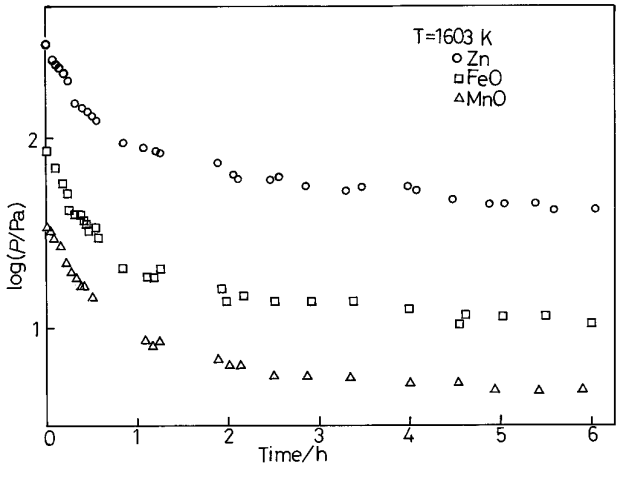

FIG. 3. Vapor pressures of Zn(g), FeO(g), and MnO(g) over the bulk sintered sample $Mn_{0.676}Zn_{0.261}Fe_{2.063}O_{4.031}$ as a function of time at 1603 K.

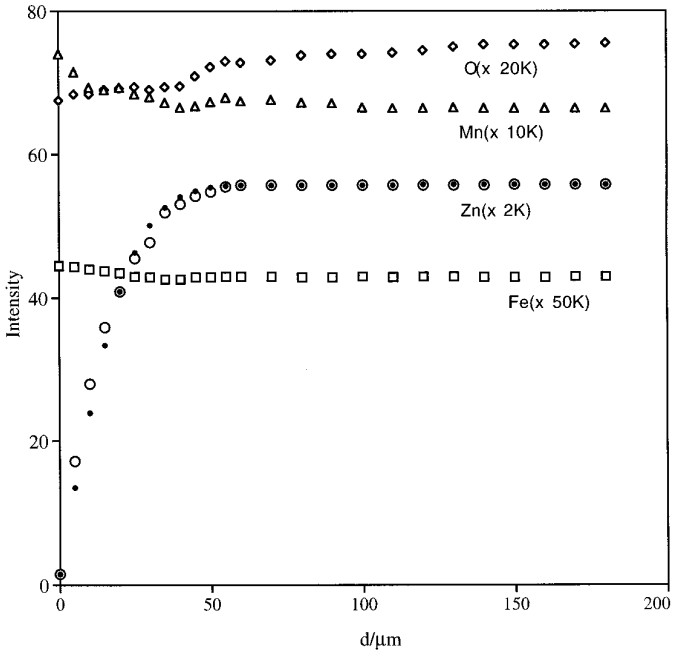

FIG. 4. Depth profiles of Zn, Mn, Fe, and O obtained from EPMA analysis of the bulk sintered sample $Mn_{0.676}Zn_{0.261}Fe_{2.063}O_{4.031}$ after evaporation for 4.5 hr at 1347 K. The dotted plot indicates the fitting points of the Zn profile according to Eq. [6].

The depth profiles of Zn, Mn, Fe, and O obtained from EPMA analysis after evaporating at 1347 K for 4.5 hr, at 1498 K for 4.5 hr, and at 1603 K for 6 hr are shown in Figs., 4, 5, and 6, respectively. The samples showing the depth profiles in Figs. 5 and 6 correspond to those showing the vapor pressure versus time curves in Figs. 2 and 3, respectively. As seen in these figures, the surface was severely depleted of Zn atoms and slightly depleted of O atoms while it was enriched with Fe and Mn atoms. As the temperature became higher, the concentration profiles of Zn, Mn, Fe, and O extended deeper zones with a smaller slope due to higher diffusivity of these atoms at higher temperatures.

IV. ANALYSIS OF DIFFUSION DATA

The diffusion behavior of Zn shown in Figs. 4–6 can be analyzed by solving the diffusion equation

$$\frac{\partial c}{\partial t} = D\,\frac{\partial^2 c}{\partial x^2}, \qquad [1]$$

where c is the concentration of Zn and x is the distance from the surface. The boundary condition for Eq. [1] may be represented as

$$c = (c_b - c_e)\exp(-\alpha t) + c_e, \quad \text{at } x = 0, t > 0 \qquad [2]$$

$$c = c_b, \quad \text{at } x \geq 0, t = 0, \qquad [3]$$

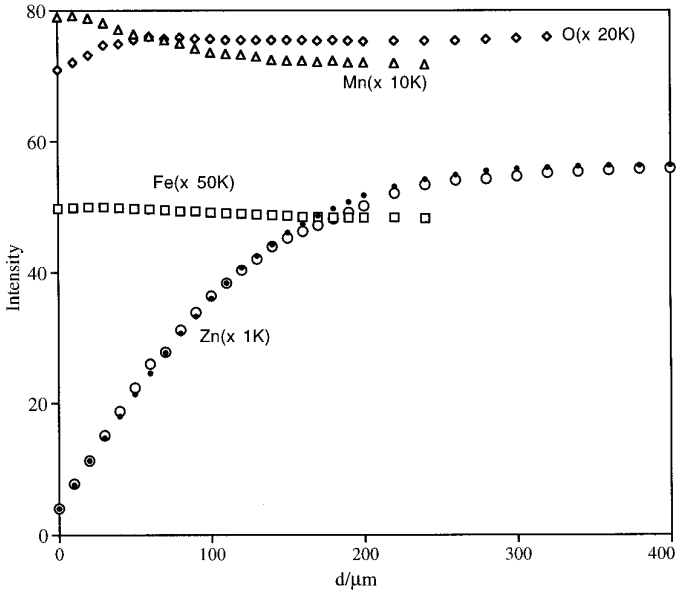

FIG. 5. Depth profiles of Zn, Mn, Fe, and O obtained from EPMA analysis of the bulk sintered sample $Mn_{0.676}Zn_{0.261}Fe_{2.063}O_{4.031}$ after evaporation for 4.5 hr at 1498 K. The dotted plot indicates the fitting points of the Zn profile according to Eq. [6].

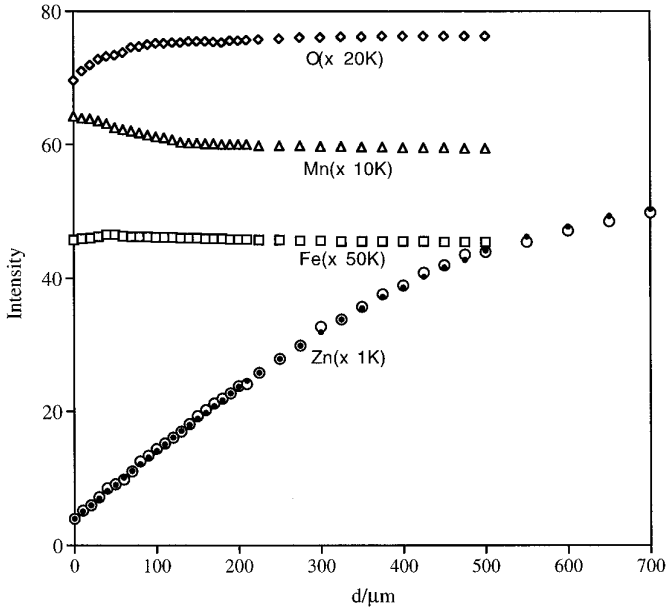

FIG. 6. Depth profiles of Zn, Mn, Fe, and O obtained from EPMA analysis of the bulk sintered sample $Mn_{0.676}Zn_{0.261}Fe_{2.063}O_{4.031}$ after evaporation for 6 hr at 1603 K. The dotted plot indicates the fitting points of the Zn profile according to Eq. [6].

where c_b and c_e are the bulk content of Zn and the surface content of Zn at infinite time, respectively. It is assumed that the surface concentration of Zn is proportional to the vapor pressure of Zn, which exponentially decreases with time as shown in Figs. 2 and 3. The Laplace transformation $\bar{c}$ of Eq. [1] using the boundary condition of Eq. [3] becomes

$$\bar{c} = \frac{c_b}{p} + c_1 \exp\left(-\sqrt{\frac{p}{D}}x\right) + c_2 \exp\left(\sqrt{\frac{p}{D}}x\right), \qquad [4]$$

where p is the parameter of the Laplace transformation. Using the boundary condition of Eq. [2] and neglecting the third term of Eq. [4] because of the finite phenomenon of diffusion behavior (11), $\bar{c}$ is represented as

$$\bar{c} = \frac{c_b}{p} + \frac{(c_b - c_e)\exp\left(-\sqrt{\frac{p}{D}}x\right)}{p + \alpha} - \frac{(c_b - c_e)\exp\left(-\sqrt{\frac{p}{D}}x\right)}{p}. \qquad [5]$$

Taking the inverse Laplace transformation of Eq. [5], c is described by

$$c = c_b + (c_b - c_e)\{1 - \exp(-\alpha t)\}\,\mathrm{erfc}\left(\frac{x}{2\sqrt{Dt}}\right). \qquad [6]$$

The depth profiles of Zn shown in Figs. 4–6 are fit to Eq. [6] assuming that c_e is zero. The parameter α is determined by fitting the surface concentration of Zn to Eq. [6], because the term $\mathrm{erfc}\{x/2(Dt)^{1/2}\}$ becomes 1 at $x = 0$. The parameter α thus determined is listed in Table 1, together with α obtained from the time dependence of the vapor pressures shown in Figs. 2 and 3. Using α thus determined, Eq. [6] is fit to the depth profiles of Zn shown in Figs. 4–6 and the diffusion constant D is determined. The theoretical Eq. [6] is also shown in Figs. 4–6 as a dotted curve. The diffusion constant thus determined is plotted as a function of inverse temperature, as shown in

TABLE 1
The Coefficient of Exponential Factors Obtained from the Time Dependence of Vapor Pressure of Zn(g) Shown in Figs. 2 and 3 and That of the Surface Zn Concentration Shown in Eq. [6]

Temperature	α obtained from vaporization data	α obtained from diffusion data
1343 K	Not available	$2.23 \pm 1.12 \times 10^{-4}$ s^{-1}
1498 K	$2.15 \pm 0.22 \times 10^{-4}$ s^{-1}	$1.63 \pm 0.82 \times 10^{-4}$ s^{-1}
1603 K	$4.45 \pm 0.45 \times 10^{-5}$ s^{-1}	$1.21 \pm 0.60 \times 10^{-4}$ s^{-1}

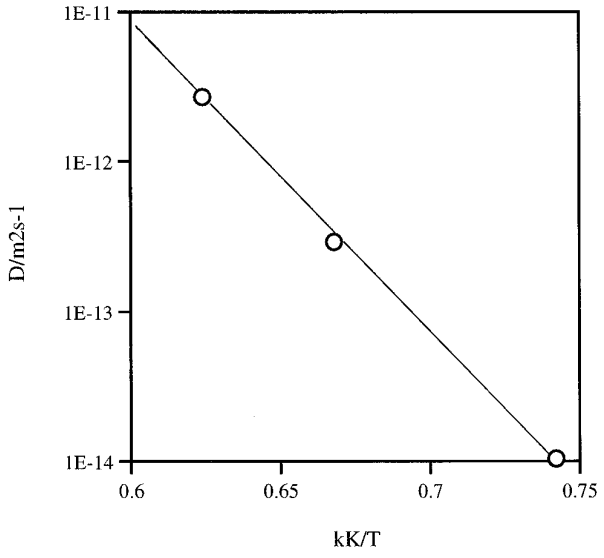

FIG. 7. Diffusion constant of Zn in the bulk sintered sample $Mn_{0.676}Zn_{0.261}Fe_{2.063}O_{4.031}$ after evaporation as a function of inverse temperature.

Fig. 7. The activation energy for diffusion is obtained as 410 kJ mol^{-1} from Fig. 7.

V. DISCUSSION

The change in the composition of Mn, Zn, Fe, and O at the surface of the powdered sample would occur during the measurement of vapor pressure, due to the predominant evaporation of Zn. It is considered to be negligibly small, however, during the measurement due to the diffusion of these atoms from the bulk resulting from the small particle size of the powder, because the vapor pressure does not change significantly during the measurement within 2 hr. When the bulk sintered sample is used, however, the vapor pressures change with time as seen in Figs. 2 and 3, since the chemical potential of each element at the surface changes with time as a result of concentrations changing by diffusion. Thus the time-dependent boundary condition of the diffusion equation is proposed as described in Eq. [2], where the surface concentration of Zn is assumed to be proportional to the vapor pressure of Zn. Strictly speaking, however, the time-dependent vapor pressure of Zn cannot be described by a single exponential function, because it appears to approach a different finite value after a longer time, as seen in Figs. 2 and 3. The reason for this phenomenon is not clear at present, but it may be due to the fact that the shape of the diffusion profiles of Fe, Mn, and O may change sharply at an initial stage and approach a steady state after a longer time as shown in Figs. 4–6. Since the vaporization reaction is considered to be fast as compared with diffusion, the time dependence of vapor pressures would represent the diffusional behavior in the bulk sintered sample. Although the magnitude of the vapor pressures is different among Zn(g), FeO(g), and MnO(g), the time dependence of their vapor pressures are quite similar, as seen in Figs. 2 and 3. This fact may result from the quite similar diffusion constants for cations in Mn–Zn ferrites as reported by Ogawa and Nakagawa (16). As seen in Figs. 2 and 3, the vapor pressures at 1498 K sharply decrease as compared with those at 1603 K. This may correspond to the sharp diffusion profile at 1498 K as compared with that at 1603 K, as seen in Figs. 5 and 6. The parameter α obtained from the initial stage in Figs. 2 and 3 is compared to that obtained from the diffusion profiles, which are listed in Table 1. Considering the large experimental error in the diffusion study, the agreement of the α parameter obtained from the two methods is rather good.

The depth profiles of Zn, Mn, Fe, and O in Figs. 4–6 show that the surface is depleted severely in Zn atoms and slightly in O atoms while, instead, it is enriched in Fe and Mn atoms. Since evaporation of Zn(g) predominantly occurs from the surface compared with MnO(g) and FeO(g), the concentrations of Mn and Fe increase relatively at and near the surface. Mn and Fe atoms diffuse against the concentration gradient according to Figs. 4–6, but they are considered to diffuse along the chemical potential gradient of Mn and Fe, since the chemical potential of Mn and Fe is considered to be decreased at the surface because of the loss of Zn. Similar up-hill diffusion was observed by Darken (17) and interpreted by Agren (18) in the Fe–Si–C system. The depletion of O atoms near the surface may be understood as due to the simultaneous vaporization of oxygen and zinc and the slowness of the diffusion of oxygen atoms as follows. As has been already described (1–6), the vaporization of Zn atoms in Mn–Zn ferrites is followed by the evaporation of oxygen as

$$\text{ZnO (in Mn–Zn ferrites)} = \text{Zn(g)} + \tfrac{1}{2}\text{O}_2\text{(g)}. \qquad [7]$$

Thus oxygen atoms as well as Zn, Mn, and Fe atoms diffuse toward the surface in order to decrease vacancies produced in both oxygen and metal sublattices. Since the diffusion constant of oxygen atoms is one or two orders magnitude smaller than that of metals (16, 19), the surface region is considered to be depleted of O atoms. As seen in Figs. 4–6, the region depleted in Zn and O atoms and enriched in Fe and Mn atoms becomes deeper as the temperature is increased. The deeper region depleted in Zn atoms would cause larger internal stress in the spinel lattice, since the lattice parameter is different between the surface and the bulk because of the different Zn concentrations between them (20). The larger internal stress may cause more severe damage in the magnetic properties.

The fitting of Eq. [6] to the profiles of Zn shown in Figs.

4–6 is thought to be satisfactory considering the assumed boundary condition shown in Eq. [2]. Among these the fit to the profile at 1347 K in Fig. 4 is relatively poor compared to those at high temperatures. The relatively poor fit at low temperatures may be due to the relatively sharp concentration change of O atoms near the surface, because the diffusion constants of cations are greatly dependent on the chemical potential of oxygen in the bulk, as suggested by the fact that the diffusion constant of cations is dependent on the partial pressure of oxygen (16). Strictly speaking, therefore, the diffusion equation must be solved under the condition that the diffusion constant is dependent on position in sample. However, such an analysis is too complicated to permit solving the diffusion equation and the diffusion constant obtained from the present study may be regarded as an apparent diffusion constant. The apparent diffusion constant thus obtained is considered to still have an important meaning from the practical point of view.

The activation energy obtained for diffusion, 410 kJ mol^{-1}, is about three times larger than the literature value, 137 kJ mol^{-1}, obtained from the tracer method (16). The larger activation energy obtained here is considered to be due to the temperature dependence of the oxygen gradient in the sample. Ogawa and Nakagawa (16) showed that the diffusion constants of Fe, Mn, and Zn became about one order of magnitude larger due to the increase of cation vacancies when the ambient partial pressure of oxygen was increased from 0.002 to 0.01 atm. At 1347 K, the depleted region of oxygen atoms extends as deep as the Zn diffuses, as seen in Fig. 4, where the number of cation vacancies are small and the diffusion constant is considered to be small. At 1603 K, however, the region depleted of oxygen atoms exists only at the surface as compared to the diffusion region of Zn atoms, as seen in Fig. 6, where the number of cation vacancies and the diffusion constant are relatively large. The larger diffusion constant at higher temperatures and the smaller diffusion constant at lower temperatures make the activation energy higher, as observed here. Thus the activation energy obtained in this study is considered to be composed of the sum of the migration energy and the energy of vacancy formation of cations, while that obtained from the tracer method includes the migration energy only (16).

VI. SUMMARY

Vapor pressures of Mn–Zn ferrites were measured by a mass-spectrometric method. The diffusion profiles were measured by EPMA and analyzed by solving the diffusion equation using the time-dependent boundary condition at the surface.

(1) Equilibrium vapor pressures were obtained using the powdered sample, where the diffusion of various atoms from the bulk to the evaporating surface was sufficiently fast. The predominant vapor species were Zn(g) with small fractions of FeO(g) and MnO(g).

(2) When the bulk sintered sample was used, the vapor pressures of Zn(g). FeO(g), and MnO(g) initially decreased with time and approached finite values. The diffusion profiles of various atoms in the same samples were analyzed by EPMA. The surface was severely depleted in Zn atoms and slightly in O atoms while it was enriched in Fe and Mn atoms.

(3) The diffusion equation is solved for the Zn profile using the time-dependent boundary condition of the surface, assuming that surface concentration of Zn is proportional to the vapor pressure of Zn. It is satisfactorily fit to the diffusion profile.

(4) From the temperature dependence of the diffusion constant thus obtained, the activation energy of diffusion was obtained at 410 kJ mol^{-1}, which is about three times larger than the literature value obtained from the tracer method. The larger activation energy obtained in this study is interpreted as due to the temperature dependence of the oxygen gradient in the sample, which includes an additional term from the vacancy formation of cations.

REFERENCES

1. T. Matsui and H. Inaba, *High Temp. High Press.* **25,** 519 (1993).
2. T. Matsui and H. Inaba, *J. Mass Spectrom. Soc. Jpn.* **41,** 335 (1993).
3. D. Condurache, C. Pasnicu, and E. Lusa, *Adv. Ceram.* **15,** 157 (1985).
4. P. Sainamthip and V. R. W. Amarakoon, *J. Am. Ceram. Soc.* **71,** 644 (1988).
5. N. J. Hellicar and A. Sicignano, *Ceram. Bull.* **61,** 502 (1982).
6. D. Condurache, C. Pasnicu, and E. Lusa, *Adv. Ceram.* **15,** 157 (1985).
7. R. Morineau and M. Paulus, *Phys. Stat. Sol. A* **20,** 373 (1973).
8. H. Inaba, *J. Am. Ceram. Soc*., in press.
9. Japanese Industrial Standards, JIS M 8213-1983 (1983).
10. Japanese Industrial Standards, JIS M 8212-1983 (1983).
11. Japanese Industrial Standards, JIS M 8215-1983 (1983).
12. Japanese Industrial Standards, JIS M 8228-1983 (1983).
13. J. B. Mann, *J. Chem. Phys.* **46,** 1646 (1967).
14. J. W. Otvos and D. P. Stevenson, *J. Am. Ceram. Soc.* **78,** 546 (1956).
15. J. Crank, "Mathematics of Diffusion." Claredon Press, Oxford, 1956.
16. S. Ogawa and Y. Nakagawa, *J. Phys. Soc. Jpn.* **23,** 179 (1967).
17. L. S. Darken, *Trans. AIME* **180,** 430 (1949).
18. J. Agren, *Metall. Trans.* **11A,** 2167 (1983).
19. H. Haneda, H. Yamamura, A. Watanabe, and S. Shirasaki, *J. Am. Ceram. Soc.* **68,** C53–C54 (1985).
20. Y. Shichijo, *Trans. Jpn. Inst. Met.* **2,** 204 (1961).